

REMOTE SENSING GEOBOTANY AND AIRBORNE GAMMA-RAY DATA APPLIED TO GEOLOGICAL MAPPING WITHIN TERRA FIRME BRAZILIAN AMAZON FOREST: A COMPARATIVE STUDY IN THE GUAPORE VALLEY (MATO GROSSO STATE, BRAZIL)

M. M. Perrotta^a, T. I. R. Almeida^b, J. B. F. Andrade^a, C. R. Souza Filho^c, G. J. Rizzotto^a, M. G. M. Santos^b

^a CPRM, Geological Survey of Brazil, Rua Costa 55, 01304-010, São Paulo, Brazil – (perrotta@sp.cprm.gov.br, jfreitas@rj.cprm.gov.br, gilmarizz@pv.cprm.gov.br)

^b Universidade de São Paulo – USP, Instituto de Geociências (IGc), Rua do Lago 562, 05508-800, São Paulo, Brasil - (talmeida@usp.br, mauricioguerreiro@uol.com.br)

^c Universidade Estadual de Campinas – UNICAMP, Instituto de Geociências (IG), Caixa Postal 6152, 13083-970, Campinas, Brasil - beto@ige.unicamp.br

KEY WORDS: Remote Sensing, Geology, Geophysics, Mapping, Forestry, Multispectral, ASTER

ABSTRACT:

This paper comprises a comparison between the vegetation response in ASTER (*Advanced Spaceborne Thermal Emission and Reflection Radiometer*) multispectral optical imagery and possibly equivalent bedrock/regolith/soil response in airborne gamma-ray spectrometry grids, employing a tropical rainforest area in the Brazilian Amazon as a control. The applied technique comprised band ratios using a fixed near infrared band (numerator) divided by individual visible and shortwave infrared bands (denominator). These band ratios were subsequently submitted to principal component analysis, and the high frequency information is smoothed by low pass filtering. The colour compositions selected for interpretation were sharpened by the first principal component of the original ASTER bands through an IHS transform in order to add albedo/texture information - lost through band rationing - back to the imagery. The products show a plausible coherence with airborne gamma-ray data and field observations, proving that the proposed processing strategy applied to low cost multispectral data can provide useful geologic information in inaccessible vegetated areas.

1. INTRODUCTION

In Amazon rainforest areas, remote sensing data (available for the whole planet and of low cost) and airborne geophysics data (of restricted availability and high cost) are the best alternative in substantiating and expanding the sparsely available ground information.

The variation of the vegetation characteristics in response to the geologic variation (geobotany) was investigated first by Agricola (1556). The author observed a clear association between poor plant growth and early plant senescence within occurrences of metallic ores. In their summary about geobotany, Ustin, *et al.* (1999) showed significant studies that demonstrate the influence of lithology, fractures and metallic mineralization in the vegetation characteristics (e.g. Chikishev, 1965; Cannon, 1960, 1971 –in: Ustin, *et al.* 1999 - and Brooks, 1972). Mouat (1982) divided the vegetation response to bedrock geochemistry in structural (physiology alteration) and taxonomic factors (set of species). Botrel *et al.* (2002) identified the relationship of soil types and topography with floristic composition and physiognomic patterns in a semi-deciduous forest in Brazil. Almeida *et al.* (2007) recognized the influence of hydrothermal alteration in vegetation distinctiveness.

Airborne gamma-ray spectrometry reflects the short wavelength (about 10^{-3} nm) gamma-ray electromagnetic radiation emitted from ground surface, related to the natural isotopic radioactive decay of K^{40} , Th^{232} and U^{238} - the last two measured by their daughters elements Tl^{208} (*eTh*) and Bi^{214} (*eU*). The gamma-ray response reflects the mineralogy of rocks, soils and regolith. Its applicability in discriminating the lithologic variation in

densely vegetated areas has proved successful in many case studies (e.g. Martelet, *et al.* 2006), despite signal attenuation coupled with high volumes of woody material and water held in the tree canopy, and signal increase due to K uptake by plants. In addition, changes in radioelements characteristics occur because of the release, redistribution, and incorporation into the regolith during weathering processes (Wilford, *et al.* 1997). In contrast, the response of rainforests in remotely sensed optical imagery is due to the interaction between the incoming solar radiation and the vegetation measured within the 400-14000 nm range. Particularly in the visible (VIS), near infrared NIR) and short wave infrared (SWIR) region (400-2500 nm), the energy reflected from the vegetation depends on trees leaves chemical composition, the plant species distribution, the canopy geometry and its health state.

Thus, since the vegetation characteristics vary partially in response to the geologic background and they can be spectrally discriminated, then this can be detected by remote sensing systems. In this context, this paper comprises a comparison between the responses of virgin tracts of forest vegetation on VIS-NIR-SWIR ASTER (*Advanced Spaceborne Thermal Emission and Reflection Radiometer*) multispectral imagery, and possibly equivalent bedrock, regolith or soil response in airborne gamma-ray spectrometry grids, employing a tropical rainforest area in the Brazilian Amazon as a control. Vegetation variation in the ASTER imagery was highlighted using an enhancement technique devised by Almeida and Souza Filho (2004).

1.1 Geological setting

The technique of vegetation spectral enhancement proposed here should be preferentially applied in areas where the native forest is preserved. Therefore, an environmental protection area (Lagoa dos Brincos Forest Reserve) was selected in the Guapore Valley, Mato Grosso state, Brazilian Amazon, for this study (fig. 1).

The regional geology comprises Cenozoic, Neogene, and Cretaceous sedimentary covers; an Ectasian basement composed of N-MORB metamafic-ultramafic rocks interleaved with banded iron formations and calc-silicate gneisses (Rizzoto, 2006). Nickel deposits are host by ultramafic, serpentinite-rich bodies; platinoid occurrences are locally associated with metamafic rocks. Thick layers of schists and paragneiss are also present. These rocks are intruded by high-K calcalkaline granitoids associated to a Mesoproterozoic intracontinental orogeny to which an amphibolite-facies regional metamorphism is observed in the area. The end of the orogeny (*ca.* 1320 Ma) was marked by the intrusion of syeno- and monzogranites. The regolith in the area comprises k-feldspar- and muscovite-bearing sediments.

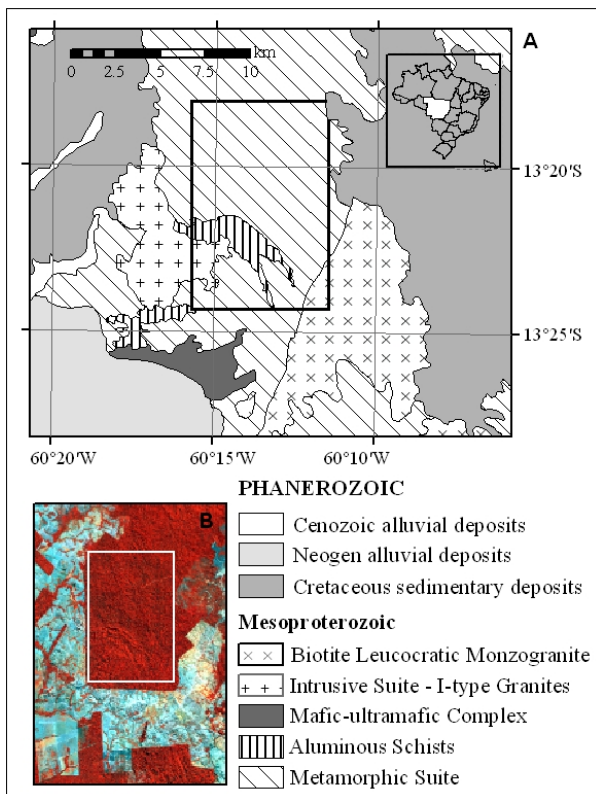


Figure 1. (A) Locality and geologic map of the study area (after Rizzoto, 2006). (B) ASTER false colour composite of bands 3,2,1 (RGB). The study area comprises the red patch in the imagery that is fully covered with natural forest.

1.2 Climate, soil and vegetation

The Guapore Valley region is located in the transition between equatorial and tropical climates. This transition is characterized by three to four drier months (June to September), strong summer rains, lowest average temperature of ~23°C and average annual precipitation of 2150 mm (Brasil/DNPM, 1979).

The study area (fig. 1) is situated in phytogeographic environment of semideciduous seasonal forest of emergent canopy (IBGE, online) developed on yellow-reddish argillaceous eutrophic soil (IBGE, online) or on rocky outcrops (Brasil/DNPM, 1979). In this environment the highest trees of the canopy have 20 to 50% of falling leaves in the drier period, although great part possess green foliage all the time, such as the shrubs and small trees of the understory. The superior stratum of this semicompact canopy has leafy cups trees that reach heights up to 20-25 m, intermixed by emerging specimens of up to 30 m. The communities established on deeper soils present higher number of individuals per hectare and greater species variation, unlike of those developed on thin, residual soil. The dominant species belong to the following families: Euphorbiaceae, Moraceae, Burseraceae, Fabaceae and Mimosaceae. Palm trees are common in humid lands and valleys. The understory is dense and obstructed by lianas that rarely involve the emerging treetops.

1.3 Vegetation organic constituents spectral characteristics relate to ASTER optical spectra

The spectral characteristics of vegetation constituents related to ASTER spectral bands can be briefly summarized as follows: the near infrared band (B3) represents the high reflectance due the leaves transparent pigments; the visible bands (B1 and B2) represent the strong absorption feature associated with photosynthetic pigments like chlorophyll-a, chlorophyll-b and carotenoids, and photoprotector or color pigments like carotenoids and anthocyanin (figure 2A); the shortwave infrared bands may register the two reflectance features associated with water content in leaf structure (B4 and B6), the absorption feature associated with starch (B5 and B6), the absorption feature related to cellulose (B7) and the absorption features related to lignin, proteins and sugars (B8) (figure 2B).

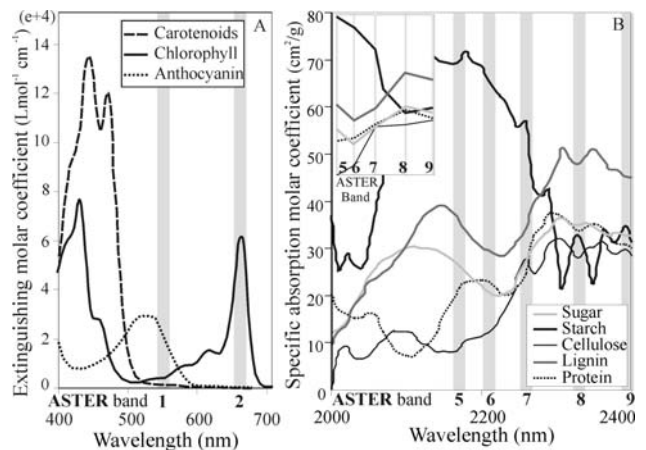


Figure 2. Absorption spectra of carotenoids, chlorophyll, anthocyanin (A); sugar, starch, cellulose, hemicellulose, lignin and protein (B) (source: Barret 1999, pers. Comm.). The inset in (B) shows the spectral signature of organic compounds at ASTER's shortwave infrared spectral resolution.

Other factors, such as anatomic structure, plant age, water availability, mineral deficiency, stress caused by chemical toxicity and parasitic attacks, can affect the optical leaves properties. Also, the canopy architecture and its health state may influence the vegetation response in optical remote sensing products. In addition, the vegetation distribution and the content

in organic constituents is strongly controlled by factors such as type of soil, topography, solar irradiation and climate gradients. This group of factors may be associated to the bedrock but the complete understanding of these relations depends on holistic studies. On the other hand, the disturbances in vegetation patterns promoted by human action or natural disasters give rise to more uncertainty in the weak geobotanical associations. In this way, the remote sensing geobotany technique is recommended to be applied in areas where the original forest is entirely preserved.

2. DATA AND METHODS

2.1 ASTER data

The ASTER VNIR and SWIR dataset used was extracted from a scene of August 4, 2001, with center coordinates at 13.5°S and 60.42°W. The three VNIR bands are centered at 0.556 μm (B1), 0.661 μm (B2) and 0.807 μm (B3), with 15 m of spatial resolution. The nine 30 m spatial resolution SWIR bands are centered at 1.656 μm (B4), 2.167 μm (B5), 2.209 μm (B6), 2.262 μm (B7), 2.336 μm (B8), 2.400 μm (B9).

The data preprocessing consists of:

- (i) SWIR bands *cross-talk* correction (ERSDAC, 2006),
- (ii) correction of the effects of atmospheric absorption and scattering on the radiance ASTER data by the use of a radiative transfer model (MODTRAN),
- (iii) SWIR bands resampling for 15 m spatial resolution (compatible with VNIR bands),
- (iv) sub-set of the work area, considering tracts covered exclusively by preserved original forest.

The applied technique for vegetation spectral enhancement (adapted from Almeida and Souza Filho, 2004) consists of:

- (v) band rationing using, like reference, a fixed near infrared band (B3) in the numerator, divided by each visible band (B1 and B2) and each shortwave infrared band (B4 to B9);
- (vi) principal component analysis (PCA) of the band ratios set, to segregate noise, to decorrelate possible redundant information and to concentrate the information of interest into some specific principal components (PCs);
- (vii) similarly, a minimum noise fraction analysis (MNF) (Green *et al.*, 1988) of the band ratios set;
- (viii) statistics and visual analysis of PCA and MNF results to determine the more representative components of the spectral variations enhanced in band ratios;
- (ix) smoothing of the high frequency information, exposed in PCA and MNF components, by 17X17 low pass filtering, for production of images of easier interpretation;
- (x) choice of smoothed PCs and MNF components for RGB color composites;
- (xi) RGB color composites sharpening by the fusion with first principal component of the original (VNIR and SWIR) ASTER bands, through a HSV (*hue, saturation, value*) transform, in order to introduce back to the imagery the albedo and texture information that was lost by band rationing.

2.2 Geophysics data

From 500 m line spaced airborne gamma-ray data (Sudeste de Rondônia project - CPRM 2007), thematic grids were generated by minimum curvature interpolation, with 125 m cell resolution, resampled to 20 m spatial resolution. These grids, as well as ASTER color composites, were sharpened by the fusion with

first principal component of the original ASTER bands, improving their ability of discrimination and localization of gamma-ray anomalies.

3. RESULTS

3.1 Vegetation spectral behavior

Pixels signatures extracted from atmospheric corrected imagery, based on color variations in B3-B1-B2 RGB color composite, show, basically, two behavior patterns (fig. 3A): curves with or without inflection feature in ASTER B4 toward B5, the first with less contrast in values between B3 and B4. Except for an evident absorption feature in B8, the SWIR bands don't show homogeneous behavior patterns.

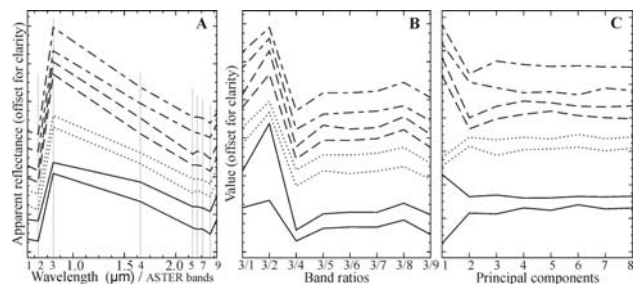


Figure 3. Vegetation pixels spectral signatures extracted from ASTER VNIR and SWIR bands set submitted to atmospheric correction (A), from band ratios set - NIR band / each VIS and SWIR bands (B), from band ratios PCs set (C). Same pixels collected in each set, symbols represent variation in behavior patterns identified in (A).

The same pixels signatures collected in band ratios set (fig. 3B) show enhancement in features related to each portion of the spectrum, but, in general, with poor distinction between curve forms. On the other hand, the same pixels collected in band ratios PCs set show strong distinction in signatures. These observations reveal the validity of the proposed technique.

3.2 Statistical results of Principal Components Analysis and Minimum Noise Fraction

The eigenvectors matrix resultant from PCA on band ratios set (table 4) shows high concentration of visible bands response in PC1, covering almost 70% of the total variation (table 5). The PC2 explains 15% of the total variation (table 5) and concentrates the shortwave infrared bands information, except for B4 strongly concentrated in PC8. The PC3, representing around 5% of the total variation, concentrates again the visible bands information but in negative correlation. Visually predominance of noise from PC4 to PC7 is noted, and, despite PC8 explaining less than 1% of the total variation, it is spatially coherent. This behavior can be explained by low covariance between B3/B4 relate to the other band ratios and its strong contribution to PC8.

In MNF analysis (eigenvalues in table 5 and eigenvectors in table 7) the contribution related to B3/B4 is again concentrated in the last component, but in opposition to PCA results, this analysis was capable to discriminate the shortwave infrared responses in different components. Because of it, a new MNF was proceeded, but in this time selecting like input the band ratios that highlight the biochemical composites more

conspicuously, B3/B2 (chlorophyll), B3/B4 (water in leaf structure), B3/B5 and B3/B6 (starch) and, finally, B3/B8 (lignin). The eigenvectors produced are shown in table 8.

R	3/1	3/2	3/4	3/5	3/6	3/7	3/8	3/9
EVc								
PC1	.41	.86	.06	.14	.14	.14	.18	.11
PC2	.31	.20	-.16	-.39	-.38	-.42	-.51	-.31
PC3	.86	-.47	.03	.06	.07	.08	.12	.06
PC4	-.02	.01	-.03	-.17	-.12	-.47	.80	-.31
PC5	.00	.00	-.03	.02	-.09	-.54	-.01	.83
PC6	.01	-.01	.08	.58	.50	-.52	-.22	-.30
PC7	-.01	.00	.06	-.67	.73	-.06	-.04	.06
PC8	.00	.00	.98	-.08	-.17	-.06	-.05	-.02

Table 4. Eigenvectors (EVc) matrix of the PCA on the set of band ratios (R). In bold the significant contributions in the PCs selected for RGB color compositions presented in figures 9A and 9B.

PC	EV %	EV cum%	MNF	EV %	EV cum%
1	72.58	72.58	1	22.52	22.52
2	18.24	90.82	2	14.02	36.54
3	4.73	95.55	3	13.00	49.54
4	1.74	97.29	4	12.20	61.74
5	1.33	98.62	5	11.50	73.24
6	0.75	99.37	6	11.27	84.51
7	0.06	99.93	7	09.97	94.48
8	0.07	100	8	05.52	100

Table 5. Eigenvalues (EV) produced in PCA and MNF analysis.

CV	3/1	3/2	3/4	3/5	3/6	3/7	3/8	3/9
3/1	.82							
3/2	1.15	2.61						
3/4	.04	.13	.03					
3/5	.11	.33	.08	.21				
3/6	.11	.33	.08	.18	.20			
3/7	.12	.35	.08	.19	.19	.25		
3/8	.15	.43	.10	.23	.23	.24	.36	
3/9	.09	.26	.06	.15	.14	.15	.18	.16

Table 6. Covariance (CV) matrix between band ratios

A series of RGB color composites were produced and sharpened for interpretation, as described in (xi) above. Three of the more representative ones are presented in figure 9. Good results were reached mainly by combinations involving PC1 or PC3, PC2 and PC8 (fig. 9A and 9B). These combinations are capable of representing the relative information to each portion of the electromagnetic spectrum and they show large color variations.

Regarding the MNF analysis of the complete band ratios group, good results were obtained in combinations between MNF3 or

MNF5, MNF7 and MNF8. A RGB color composite based on the result of the MNF analysis of the selected band ratios is presented in figure 9C, the components that had been used were MNF1, MNF4 and MNF5, the first and the last in their negative form, what sometimes bring more useful color composites. In figure 9 it is also shown three aerogeophysics grids ϵ Th, K and ternary (K-U-Th) RGB radiometric map, all of them sharpened through a HSV fusion with the first PC of the VNIR-SWIR ASTER set allocated in the value channel.

R	3/1	3/2	3/4	3/5	3/6	3/7	3/8	3/9
EVc								
1	.28	-.35	.15	-.03	-.15	.01	-.30	.81
2	.44	-.18	.20	.23	.24	.23	.75	.06
3	.02	-.02	.00	.28	.80	-.48	-.22	.06
4	-.14	-.05	-.03	.69	.05	.63	-.32	-.01
5	-.36	.42	-.21	.38	-.22	-.32	.38	.45
6	-.39	.15	-.13	-.48	.48	.46	.14	.34
7	.60	.76	-.04	-.10	.04	.09	-.17	.07
8	-.25	.23	.93	-.01	-.01	-.03	-.03	.01

Table 7. Eigenvectors (EVc) matrix of the MNF analysis on the set of band ratios (R)

R	3/2	3/4	3/5	3/6	3/8
EV					
1	-.27	.38	.10	-.35	.80
2	.37	-.29	.40	-.77	-.11
3	-.12	.00	.90	.41	.02
4	-.45	.59	.09	-.32	-.58
5	.74	.65	.03	.14	.00

Table 8. Eigenvectors (EV) matrix of the MNF analysis on the set of band ratios (R) 3/2, 3/4, 3/5, 3/6, 3/8. In bold the significant contributions in the MNF selected for RGB color compositions presented in figure 9C.

4. DISCUSSION

All the generated products, either by manipulation of ASTER imagery or by the improvement of aerogeophysics grids, point to a larger lithologic complexity of the study area than the introduced in the preliminary geological map. A sketch of interpretation of the data (fig. 10A) was accomplished in GIS environment so that all images could be evaluated together. For larger coherence of the drawn contacts, linear features extracted from the PC1 were also incorporated.

Given the series of factors that influence the spectral behaviour of the vegetation, such as the soil, terrain topography, heatstroke, readiness of water and the own rocky substratum, it is noted that in ASTER processed images different lithologies can present similar signatures, and not always similar signatures represent the same lithology. Because of it, the appropriate interpretation of these images should be based on tonal contrasts, always associating the textural data and topographical and field observations.

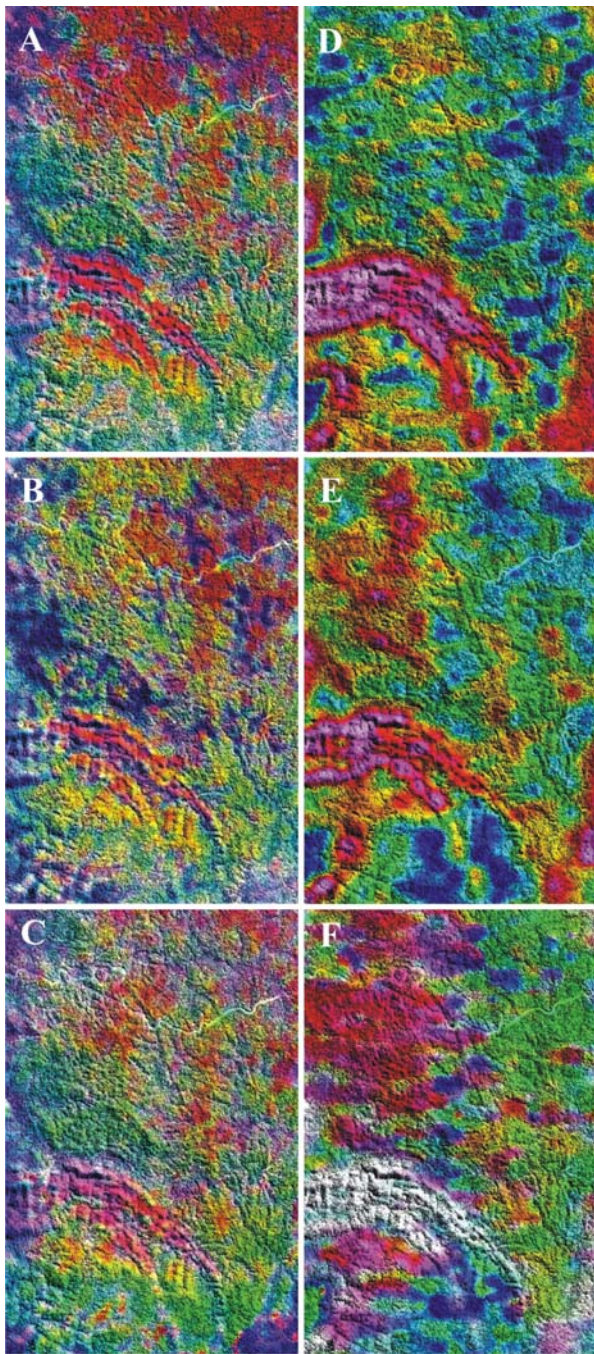


Figure 9. (A, B, C) Images generated by PC and MNF analysis from band ratios. The components were filtered by 17X17 low pass filter and the color composites were sharpened by HSV transform with PC1 of the original ASTER bands in value channel. (A) and (B): ratios B3/each of all others; (C): ratios 3/2, 3/4, 3/5, 3/6 and 3/8. (A) PC1, PC8, PC2 in RGB. (B) PC1, PC3, PC2 in RGB. (C) (-MNF1), (-MNF5), MNF4 in RGB. (D, E, F) Aerogeophysics grids sharpened by HSV transform with ASTER original bands PC1 in value channel. (D) *eTh* channel, (E) K channel, (F) ternary (K-U-Th) radiometric map.

As noticed in figure 9, there are several coincidences among the ASTER imagery processed and the gamma-ray grids. As a more outstanding feature the fold in the central-southwestern portion is evident in all generated images, corresponding to the high radiometric signature in all gamma-ray themes, identified by magenta and reddish colours in *eTh* and K grids (fig 9C and

9D), and white in ternary (K-U-Th) RGB radiometric map. According to field data, in the prolongation to the west of this structure, and in lenses of similar radiometric signature northwestwards (fig. 10B), the lithologic content of this geologic unity can be described as aluminous schist.

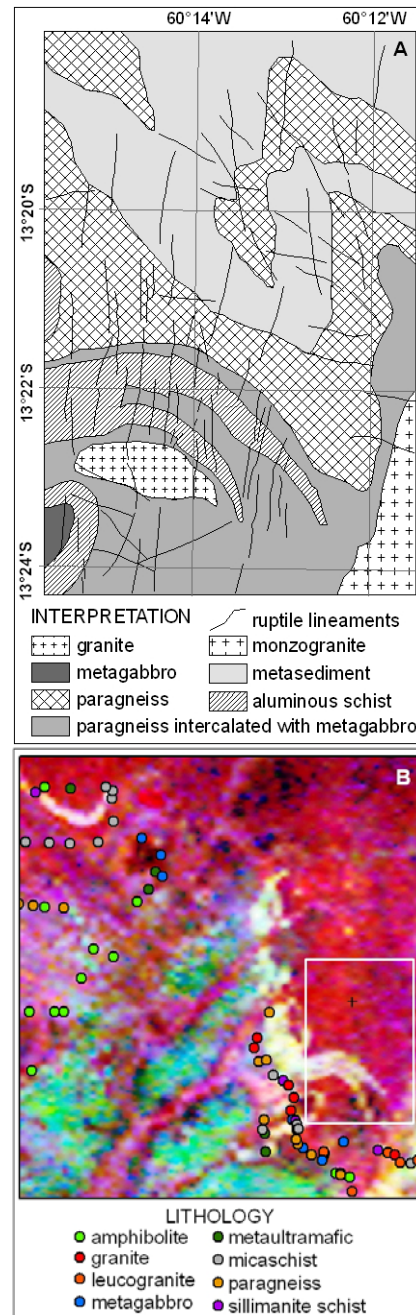


Figure 10. Interpretation based on images and outcrop data (A). Aerogeophysics, ternary radiometric map (RGB=K-Th-U) with lithologic data of outcrops (B).

The ASTER products suggest that these lenses have more restricted thicknesses than it could be interpreted by the geophysics, and they occur as intercalations in predominant metamorphic rocks in the area. Wilford *et al.* (1997) describe signatures relatively high in the channels K, *eTh* and *eU* in argillaceous regolith derived from schists and phyllite in the west of Australia. The element K would be associated with clay

minerals and micas while Th and U would occur associated with clay minerals, oxides of Iron or Titanium and lithic fragments. The presence of anatexis in these rocks can not be discarded, since they reach the sillimanite zone metamorphism. This could explain the high relief, because of the widespread presence of granitic veins, and a compatible radiometric behavior with granitic rocks in the gamma-ray data. On the other hand, the more accentuated relief can indicate rocks closer to the surface, what would elevate, relatively, the radiometric values, in spite of the topographical correction, applied to the rude gamma-ray data. South of this feature the presence of a granitic body is suggested by the tonal variations in ASTER processed images, high relief, and high signature in the channel K, moderate in the channels Th and U and low in the ratio eU/eTh , a behaviour similar to the latest phases in the magmatic evolution (Dickson & Scott, 1997). The unit mapped as metamorphic suite (fig. 1) associated with schists and paragneiss, has moderate and heterogeneous signatures among the geophysical themes in the central-northern portion of the area. However, in the ASTER images, such as in the gamma-rays grids, subdivisions can be sketched being organized in a wide fold with NW orientation axial trace (fig. 10A). In the southwestern corner, a metamafic body (also suggested in adjacent field data – fig. 10B) is well delimited in geophysical images, outlined by probable aluminous schist. In southeastern portion, the relative high radiometric signature in channels K, eTh and eU indicate the presence of the mapped biotite monzogranite, also evident in the color composites (figures 9A, 9B and 9C).

It is important to mention that, in the west edge of the area, close to the deforested region, an alteration in spectral signal can be due to residual cross-talk effects (ERSDAC, 2006) that mainly affect features separated by abrupt variation of signal.

5. CONCLUSION

The results of this work show the plausible coherence between the processed ASTER products, airborne gamma-ray data and field observations, proving that the proposed processing strategy applied to low cost multispectral data can provide useful geologic information in inaccessible vegetated areas mainly for which no airborne geophysical data are available.

REFERENCES

- Agricola, G., 1556. *De Re Metallica*. Froben, Basileae. Translated from Latin by Hoover, H.C. & Hoover, L.H. 1912. Dover Publications, Inc., New York, 1986. 640 p. http://www.farlang.com/gemstones/agricola-metallica/page_001 (accessed 15 Feb. 2008)
- Almeida, T.I.R. & Souza Filho, C.R., 2004. Principal component analysis applied to feature-oriented band ratios of hyperspectral data: a tool for vegetation studies. *International Journal of Remote Sensing*, 25, pp. 5005-5023.
- Almeida, T.I.R., Juliani, C., Mantovani, W., Perez-Aguilar, A., 2007. Comunidades florestais como indicadores geobotânicos: o caso da mineralização aurífera do Grupo Serra do Itaberaba, Guarulhos, São Paulo. *Revista Brasileira de Geociências*, 37(1), pp. 37-49.
- Botrel, R.T., Oliveira Filho, A.T., Rodrigues, L.A., Curi, N., 2002. Influência do solo e topografia sobre as variações da composição florística e estrutura da comunidade arbóreo-arbustiva de uma floresta estacional semidecidual em Ingai, MG. *Revista Brasileira de Botânica*, 25(2), pp. 195-213.
- Brasil/DNPM-Departamento Nacional de Produção Mineral, 1979. *Projeto RADAM: folha SD-20 Guaporé, Levantamento de Recursos Naturais*, Vol.19, 369 pp.
- Brooks, R.R., 1972. *Geobotany and Biogeochemistry in Mineral Exploration*. Harper & Row, New York, 290 pp.
- CPRM – Geological Survey of Brazil, 2007., Projeto Aerogeofísico Sudeste de Rondônia (RO-MT). Magnetometria e Gamaespectrometria. Code 1068. Base de metadados AERO. <http://www.cprm.gov.br/aero/aero.htm>. (accessed 2 Jul. 2007).
- Dickson, B.L. & Scott, K.M., 1997. Interpretation of aerial gamma-ray surveys-adding the geochemical factors. *AGSO Journal of Australian Geology & Geophysics*, 17, pp. 187-200.
- ERSDAC - Earth Remote Sensing Data Analysis Center, 2006. *Aster product guide. Release Note (updated on 3/10/2006)*. http://www.gds.aster.ersdac.or.jp/gds_www2002/service_e/release_e/set_release_ecrs.html. (accessed 2 Jul. de 2007).
- Green, A. A., Berman, M., Switzer, P., Craig, M. D., 1988. A transformation for ordering multispectral data in terms of image quality with implications for noise removal. *IEEE Transactions on Geoscience and Remote Sensing*, 26: pp. 65-74.
- IBGE-Instituto Brasileiro de Geografia e Estatística, *Online*. Banco de dados georreferenciado, folha SD-20: vegetação. ftp://geoftp.ibge.gov.br/mapas/banco_dados_georeferenciado_recursos_naturais/latlong/SD-20/vegetacao.exe. (accessed 29 Nov 2007)
- Martelet, G., Truffert, C., Tourlière, B., Ledru, P., Perrin, J., 2006. Classifying airborne radiometry data with agglomerative hierarchical clustering: a tool for geological mapping in context of rainforest (French Guyana). *International Journal of Applied Earth Observation and Geoinformation*, 8, pp. 208-223.
- Mouat D.A. 1982. The response of vegetation to geochemical conditions. In: *International Symposium on Remote Sensing for Exploration Geology, Proceedings, 2nd Thematic Conference*, pp. 75-84.
- Rizzotto G.J. 2006. Geologia da Folha Pimenteiras (SD.20.X.D), região limítrofe Brasil-Bolívia. In: *SBG, Congresso Brasileiro de Geologia, 43, Anais*, pp. 189.
- Ustin, S.L., Smith, M.O., Jacquemoud, S., Verstraete, M.M., Govaerts, Y.M., 1999. Geobotany: Vegetation Mapping in Earth Sciences. In: Rencz A. N. (ed.) *Remote Sensing for Earth Sciences: Manual for Remote Sensing* (vol. 3), 3rd ed. John Wiley & Sons Inc., New York, USA, pp. 189-247.
- Wilford, J.R., Bierwirth, P.N., Craig, M.A., 1997. Application of airborne gamma-ray spectrometry in soil/regolith mapping and applied geomorphology. *Journal of Australian Geology & Geophysics*, 17, pp. 201-216.